




# Numerical investigation of saturated upward flow boiling of water in a vertical tube using VOF model: effect of different boundary conditions

B. Hasanpour<sup>1</sup> · M. S. Irandoost<sup>1,2</sup> · M. Hassani<sup>1</sup> · R. Kouhikamali<sup>1</sup> 

Received: 6 August 2017 / Accepted: 10 January 2018 / Published online: 23 January 2018  
© Springer-Verlag GmbH Germany, part of Springer Nature 2018

## Abstract

In this paper a numerical simulation of upward two-phase flow evaporation in a vertical tube has been studied by considering water as working fluid. To this end, the computational fluid dynamic simulations of this system are performed with heat and mass transfer mechanisms due to energy transfer during the phase change interaction near the heat transfer surface. The volume of fluid model in an available Eulerian-Eulerian approach based on finite volume method is utilized and the mass source term in conservation of mass equation is implemented using a user defined function. The characteristics of water flow boiling such as void fraction and heat transfer coefficient distribution are investigated. The main cause of fluctuations on heat transfer coefficient and volume fraction is velocity increment in the vapor phase rather than the liquid phase. The case study of this research including convective heat transfer coefficient and tube diameter are considered as a parametric study. The operating conditions are considered at high pressure in saturation temperature and the physical properties of water are determined by considering system's inlet temperature and pressure in saturation conditions. Good agreement is achieved between the numerical and the experimental values of heat transfer coefficients.

**Keywords** VOF model · Finite Volume Method · User defined function · Vertical tube · Two-phase flow · Convection heat transfer · Vapor void fraction

## Nomenclature

$c_l, c_g$  Empirical coefficients used in Eq. 12, 13 (1/s).  
 $D$  Diameter (m).  
 $E$  Enthalpy (J/kg).  
 $\vec{F}_\sigma$  Volumetric surface tension force (N/m<sup>3</sup>).  
 $\vec{g}$  Gravitational acceleration (m/s<sup>2</sup>).  
 $h$  Convective heat transfer coefficient (W/m<sup>2</sup>-K).  
 $h_{lg}$  Latent heat (J/kg).  
 $k$  Curvatures of phases.  
 $k_e$  Effective thermal conductivity (W/m-K).  
 $L$  Length (m).  
 $P$  Pressure (Pa).  
 $\dot{Q}$  Heat transfer rate source term (W/m<sup>3</sup>).

$S$  Mass source term (kg/m<sup>3</sup>-s).  
 $T$  Temperature (K).  
 $t$  Time (s).  
 $\vec{u}$  Velocity field (m/s).  
 $z$  Axial location (m)

## Greek symbols

$\sigma$  Interfacial surface tension (N/m).  
 $\alpha$  Volume fraction.  
 $\rho$  Density (kg/m<sup>3</sup>).  
 $\mu$  Viscosity (kg/m-s)

## Subscripts

$l$  Related to the liquid phase.  
 $g$  Related to the vapor phase.  
 $sat$  Saturation.

✉ R. Kouhikamali  
kouhikamali@guilan.ac.ir

<sup>1</sup> Department of Mechanical Engineering, University of Guilan, P. O. Box 3756, Rasht, Iran

<sup>2</sup> School of Mechanical Engineering, University of Tehran, P. O. Box 11365-4563, Tehran, Iran

## 1 Introduction

Heat transfer mechanisms related to the interaction of liquid–vapor phase change play an important role in two-phase flow evaporation. Two-phase flow in a tube has become important

for compact heat exchanger applications such as evaporators in recovery boilers. They are mainly used due to their high efficiency, smaller volume, improved safety and power savings compared to other kinds of conventional heat exchangers. Furthermore, understanding of two-phase flow evaporation can possibly decrease manufacturing costs, energy consumption and subsequently leads to performance improvement.

The numerical investigation of two-phase flow boiling of refrigerant R141B was conducted inside a horizontal coiled tube, whereas the temperature profile was meaningfully influenced by phase change characteristics and higher temperatures in vapor region [1]. It was revealed that due to the interaction of two phase flow with interface of liquid-vapor phases, the flow velocity difference between the two phases depends on the phase change distribution. An analysis of heat transfer was implemented based on tube length calculation for the sub-cooled flow boiling regions in which an optimized function of heat transfer coefficient was found to be dependent on tube length [2]. Numerical simulation of boiling two-phase flow using the VOF (Volume of Fluid) method in a micro-channel was carried out by Fang et al. [3]. The goal was to provide optimization of vapor-venting heat exchangers performance in which effects of the membrane condensation and surface wettability were discussed. Furthermore, an analysis of temperature profile, pressure drop and two-phase flow patterns were implemented to supply a comparison between the vapor-venting channel and the conventional channel. A numerical approach of bubble behaviors in sub-cooled flow boiling of water based on the VOF method had been conducted by Wei et al. [4] considering energy and mass transfer during phase change. The behaviors of bubble sliding, coalescence, detachment and bubble shape variation in an upward vertical, rectangular channel under the effect of inertial forces were investigated in different pressure and heat flux. Besides, the pressure, velocity vector and temperature distribution around two isolated bubbles were studied near the heated wall. A research is implemented by Kouhikamali et al. [5] based on two-phase flow evaporation in thermal systems with heat exchangers. The characteristics of water flow boiling were analyzed in the range of various heat fluxes. The numerical simulation of transient solution such as void fraction, heat transfer coefficient and wall temperature distribution were investigated in an upward vertical tube. The effect of fluctuations behavior on volume fraction, heat transfer coefficient and wall temperature was discussed due to energy and mass transfer during phase change and liquid-vapor interface on the heated wall. The average of heat transfer coefficient on the heated wall was compared with experimental result and a good agreement was found. A numerical investigation of heat and mass transfer and flow characteristics of evaporation and condensation process for the films flowing on both the inner and outer fluted tube wall was investigated by Park and Seouk [6]. The transport equations for momentum and energy were solved by

using the finite volume method (FVM) and the velocity and temperature fields were studied for various flute shapes. FVM uses the transport equations of momentum and energy. Chen et al. [7] numerically studied the adapted flow pattern for upward flows using phase separation concept. VOF model was carried out to recognize the mechanisms for heat transfer enhancement. Ma and Bothe [8] studied different velocities at the interface which happens due to phase change. In their simulation, heat transfer mechanism was based on a two-scalar approach where two different temperature fields were utilized for the temperature inside the two phases. Ratkovich et al. [9] investigated a vertical two-phase gas-liquid flow. Two-phase slug flow was studied using CFD and the results were compared with both experimental and empirical assessments. Good agreement between the CFD results and the experimental and empirical ones was obtained. In another study by Meng et al. [10] boiling flow of refrigerant R141b in both inclined and vertical serpentine tubes was investigated. CFD code was used to simulate the flow and heat transfer. They indicated that the simulated flow pattern was in good agreement with the experimental one. Liu et al. [11, 12] studied vertical upward two-phase annular flow numerically. They improved a new two-fluid CFD model to investigate the wave flow. Their proposed model could provide details about gas core and film flows and their interactions. Ramirez et al. [13] studied two-phase flow and heat transfer in horizontal tubes. The tubes were fitted with baffles of vertical cut. A simplified model was developed for stratified flow. Their model improved the prediction of heat transfer in exchangers fitted with vertically cut baffles. Maqbool et al. [14] studied two phase heat transfer and pressure drop of propane in a circular minichannel. It was concluded that the heat transfer coefficient increases with an increase in heat flux and saturation temperature while the influence of mass flux and vapor quality was insignificant. Chiapero et al. [15] experimentally studied boiling heat transfer coefficient of R134a for two different mass fluxes and heat fluxes. It was revealed that increasing mass flux enhances heat transfer mainly at high vapor fractions while increasing heat flux enhances heat transfer mostly at low vapor fractions. Chen et al. [7] numerically investigated flow patterns for a vertical upflow using CFD. It was shown that void fraction, velocity of phases and liquid film thickness in annular region were essential for increment in heat transfer. Tsui and Lin [16] modeled fluid dynamics and heat transfer of phase change flows with an algorithm based on VOF method. In their study, the interface between the two fluids was represented by a continuous surface as the contour surface of the VOF function. Hardt and Wondra [17] studied vapor-liquid flow using an evaporation model that incorporates an evaporation source-term derived from a physical relationship for the evaporation mass flux. Recently a VOF-based method was conducted by Pan et al. [18] in which the vapor and liquid phases were distinguished using a color function representing

the local volume fraction of the tracked phase. In this method, the source terms were coupled with the local temperature explicitly which led to a reduction in computational cost. Kafeel and Turan [19] investigated steady state operation of a vertical two phase thermo-syphon using the two-fluid technique. The effects of evaporation, condensation and interfacial heat and mass transfer were studied in the domain and it was shown that this method can effectively be used for simulation of two phase flow systems. An improved VOF model based on Navier-stokes equations for multiphase flows is developed by Lorstad and Fuchs [20]. The VOF model was carried out for different flow types at low Reynolds numbers and for path-oscillating bubbles. Their numerical simulations were in agreement with experimental results quantitatively. Das and Das [21] modeled gas-liquid phase change with an algorithm based on smoothed particle hydrodynamics. The model was utilized to simulate vapor formation around solid spheres. Their simulation showed good agreement with available present literature.

The present work describes parametric study for different tube diameters and fin size of tube bundle inside a heat recovery steam generator (HRSG) systems. A simulation model of two phase flow evaporation is presented due to the need for high quality water and vapor in power plants. The work is divided into two main investigations conducted for investigation of tube diameter and fin size on evaporator tube bundle to improve the performance of HRSG systems. The first investigation presents the effect of fin size extension on the finned tube which is based on convection boundary conditions. Another main investigation is directed on the performances of tube size which is based on the arrangement of tube bundles. The main purpose of this work is to investigate and simulate sub-cooled and saturated two-phase flow boiling when the upward saturated water flow is evaporated inside the tube through exhaust gases of a gas turbine. A parametric study of volume fraction and heat transfer coefficient on the convection boundary condition and tube diameter variations is conducted numerically. The investigation is based on an industrial need for HRSGs and by changing tube fin size and its diameter, the desired and optimum percentage of vapor volume fraction can be determined in the tube. The goal of the study is to investigate volume fraction of vapor inside the tube locally through the tube in axial direction in different time instants as well as in different boundary conditions. Furthermore, this study addresses the unsteady nature of the flow and its main focus is on vapor void fraction in tube. The oscillatory pattern of the flow as well as volume average of vapor void fraction variations with time through the tube is studied.

## 2 Multiphase flow description

There are three significant regions inside an evaporation tube named compressed pure liquid region, sub-cooled

flow region in which primary bubbles is formed on the heated surface and saturated two-phase flow region [22]. The liquid temperature in sub-cooled flow region is less than saturation temperature. In this study it is assumed that the saturation temperature is constant along the tube. There are numerical simulations of water flow as working fluid at high pressure for evaporation of two-phase flows. Two-phase flows with phase change are extremely affected by the exchange of mass and momentum and the characteristics of interfacial tension forces between the liquid and vapor phases in the flow.

Generally there are three steps of modeling approach for the multiphase flow regimes. The first step is an interpretation of phase number. The second step contains analysis of the conservation of mass, momentum and energy equations in control volume. Finally, the last step includes solution of governing equations describing numerical simulation of multiphase flows.

### 2.1 Governing equations

#### 2.1.1 Mass conservation equation (Interface tracking of volume fraction)

In the VOF model, tracking of the surface between the phases is solved by conservation equations and the equations are solved for the volume fraction of one of the phases. The analysis for two-phase flow does not explicitly trace the interface [23–25]. An interpretation of the terms in the mass conservation equation can be written in the form of Eqs. (1) and (2):

$$\frac{\partial \alpha_l}{\partial t} + \vec{\nabla} \cdot (\vec{u} \alpha_l) = \frac{-S}{\rho_l} \quad (1)$$

$$\frac{\partial \alpha_g}{\partial t} + \vec{\nabla} \cdot (\vec{u} \alpha_g) = \frac{S}{\rho_g} \quad (2)$$

in which  $\alpha_l$  and  $\alpha_g$  denote the volume fraction of the liquid phase and vapor phase, respectively. The summation of volume fractions of both phases is unity. The first and the second term at the left-hand side represents accumulation and the contribution of convection, respectively. The mass source,  $S$  ( $\text{kg}/(\text{m}^3\text{s})$ ) depicts the sum of volumetric sources of all the phases as a user-defined source term due to phase change.

#### 2.1.2 Momentum conservation equation

In accordance with the Navier-Stokes formulations and the interfacial two phase flow, the momentum transport equations in cells are solved for only one of the two phases. The momentum equation depends on the volume fractions of all

phases, and the force caused by the surface tension must be taken into account at the interface.

$$\frac{\partial}{\partial t} (\rho \vec{u}) + \nabla \cdot (\rho \vec{u} \vec{u}) = -\nabla p + \nabla \cdot \left[ \mu \left( \nabla \vec{u} + \nabla \vec{u}^T \right) \right] + \rho \vec{g} + \vec{F}_\sigma \tag{3}$$

In this equation  $\vec{F}_\sigma$  is the volumetric surface tension force employing the Continuum Surface Force (CSF) model proposed by Brackbill et al. [26] and  $\vec{u}$  represents the shared velocity field while  $p$  is the pressure and  $\rho \vec{g}$  is the gravitational force. The averaged properties of density  $\rho$  and viscosity  $\mu$  are shared by the phases according to the following forms:

$$F_\sigma = \sigma \frac{\alpha_l \rho_l k_g \nabla \alpha_g + \alpha_g \rho_g k_l \nabla \alpha_l}{0.5(\rho_l + \rho_g)} \tag{4}$$

$$\rho = \alpha_l \rho_l + (1 - \alpha_l) \rho_g \tag{5}$$

$$\mu = \alpha_l \mu_l + (1 - \alpha_l) \mu_g \tag{6}$$

where  $\sigma$  (N/m), the interfacial surface tension between the phases can be written in terms of the pressure jump across the surface and acts as the source term in the momentum equation.  $\rho_l$ ,  $\rho_g$ ,  $k_l$  and  $k_g$  are also the liquid density, vapor density and the curvatures of the liquid and vapor phases, respectively. The curvatures of the phases used to adjust the body force term in the surface tension calculation are represented as:

$$k_l = \frac{\nabla \alpha_l}{|\nabla \alpha_l|}, \quad k_g = \frac{\nabla \alpha_g}{|\nabla \alpha_g|} \tag{7}$$

As previously discussed, the VOF model simulates the motion of different phases by tracking the motion of the interface throughout the solution domain. The tracking of interface between the phases is carried out by solving a continuity equation for the volume fraction of each phase when a control volume is not entirely filled by one phase.

### 2.1.3 Energy equation

The form of energy equation shared between the liquid and vapor phases is represented as:

$$\frac{\partial}{\partial t} (\rho E) + \nabla \cdot [\vec{u} (\rho E + p)] = \nabla \cdot (k_e \nabla T) + \dot{Q} \tag{8}$$

where,  $T$ ,  $E$  and  $k_e$  are the shared temperature field, enthalpy and the effective thermal conductivity, respectively. The

source term  $\dot{Q}$  ( $W/m^3$ ) includes the heat transfer rates through the interface.

$$E = (\alpha_l \rho_l E_l + (1 - \alpha_l) \rho_g E_g) / (\alpha_l \rho_l + (1 - \alpha_l) \rho_g) \tag{9}$$

$$k_e = \alpha_l k_{e,l} + (1 - \alpha_l) k_{e,g} \tag{10}$$

where,  $E_l$  and  $E_g$  are concluded based on the specific heat of liquid and vapor phases explained by:

$$E_l = C_l(T - 298.15), \quad E_g = C_g(T - 298.15) \tag{11}$$

## 2.2 Phase change considerations

### 2.2.1 Mass transfer source term

In order to simulate the evaporation process from liquid to vapor phase, mass transfer modeling is adapted [4]. The phase change is performed at a constant pressure and the saturation temperature is based on the mass source term. Saturation occurs at  $T \geq T_{sat}$ . The mass transfer rate of the phase change in the control volume of the liquid phase and the vapor phase decreases and increases, respectively. The magnitude of mass source term can be followed as:

$$S = c_l \alpha_l \rho_l \frac{T - T_{sat}}{T_{sat}} \tag{12}$$

Condensation occurs at  $T \leq T_{sat}$ . The mass transfer rate of the phase change in the control volume of the liquid phase and the vapor phase increases and decreases, respectively. The magnitude of mass source term is represented as:

$$S = c_g \alpha_g \rho_g \frac{T - T_{sat}}{T_{sat}} \tag{13}$$

In order to acquire a good agreement of the numerical convergence of the interfacial temperature at  $T_{sat}$ , the empirical coefficients  $c_l$  and  $c_g$  are predicted by the model and the experiments. In addition, the large values of  $c_l$  and  $c_g$  causes numerical convergence problem, and the small values lead to a meaningful inconsistency of the temperature accuracy near the interfaces [1]. It was noticed that beside these restrictions, the continuity and energy equations' convergences depend on this value and the relating balances are good keys for the selection of this value. Therefore in the current study, the value of  $c_l$  and  $c_g$  are found out to be  $10 \text{ s}^{-1}$ . They have a converged solution with the lowest deviation from saturation temperature at the interface and the best convergences of continuity and energy equations by try and error.

## 2.2.2 Heat transfer source term

The evaporation and condensation mass transfer source term is derived from the heat transfer source term. The heat transfer source could be directly achieved by:

$$\dot{Q} = S \cdot h_{lg} \quad (14)$$

where  $\dot{Q}$  represents the phase change caused by energy transfer and is calculated from the mass transfer source of evaporation  $S$  and the latent heat  $h_{lg}$ .

## 3 Numerical method and simulations

### 3.1 Geometrical considerations and operating conditions

The computational non-uniform domain of tube geometry is depicted in Fig. 1. The computational grid of domain is divided into structured quadrilateral cells [5]. In order to assure an accurate simulation of the phenomena occurring near the tube wall region, layers of cells are placed as the enhanced wall function [27]. The flow direction is upward and the influence of gravitational acceleration has been taken into account. The inlet and outlet boundary conditions are considered as mass flow inlet and pressure outlet, respectively. The heated wall is also employed by the convection boundary condition.

### 3.2 Solution methodology and convergence criterion

Due to the dynamic behavior of fluid flow, a transient simulation of two-phase flow evaporation with a variable time step size is executed. The conservation equations are solved according to the VOF model in *ANSYS Fluent 6.3* code with a UDF as a source term. The considered UDF is developed exactly according to the Eqs. 12–14 in C programming language. This UDF, according to the computed cells' temperature and properties, determines the source terms of continuity and energy equations. The values of the source terms are updated every iteration after computing temperature and are used in relations in the next iteration. In order to improve the computational efficiency, there are two corrections containing neighbor correction and skewness correction for PISO algorithm in comparison with the SIMPLE and SIMPLEC algorithms [28]. Spatial discretization of the continuity and volume fraction equations is carried out by applying the Pressure Staggering Option (PRESTO) and the modified High Resolution Interface Capturing (HRIC) scheme, respectively. Modified HRIC scheme is classified into the color-function volume of fluid and used high resolution scheme for discretization of convection term in transport equation. The second-order upwind calculation scheme is utilized in momentum, energy, and the two turbulent equations [29]. Transient simulations are performed until a steady-state condition is obtained. In order to ensure solution stability, the time step is adjusted to maintain the Courant-Friedrichs-Levy (CFL) number  $\frac{U_{\max} \cdot \Delta T}{\Delta x}$  of 0.1.

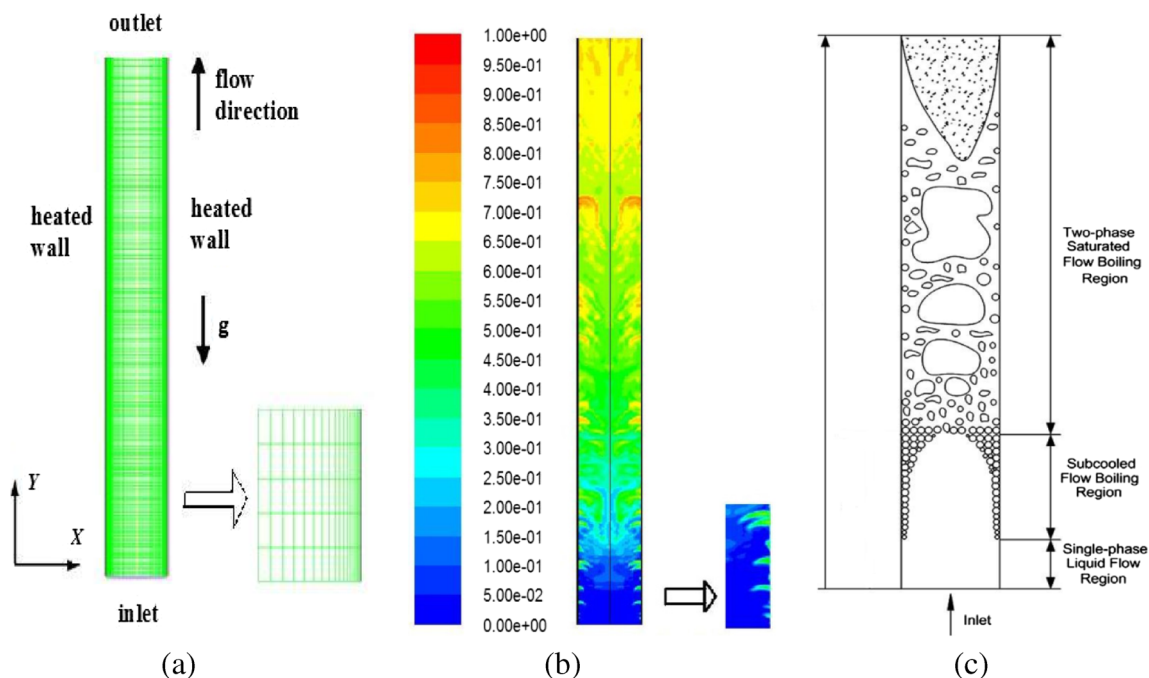


**Fig. 1** Two-phase flow during upward flow boiling in a vertical tube (a) Schematic diagram of computational domain (b) Contour of vapor volume fraction (c) Two-phase flow regimes during evaporation

### 3.3 Turbulence modeling

In this investigation, the simulation is considered as turbulent flow based on the Shear-Stress Transport (SST)  $K - \omega$  model, wherein a modified formulation of the standard  $K - \omega$  model is adopted to take the SST effects into account. This model was developed by Menter [30] to efficiently blend the strong and precise formulation of the  $K - \omega$  model in the near-wall region and the  $K - \epsilon$  model in the far field. The local turbulent viscosity is concluded from the solution of transport equations for the turbulent kinetic energy,  $K$  and the energy dissipation rate,  $\omega$ . The turbulence boundary layer near the wall includes a thin laminar sub-layer adjacent to the wall and a ‘buffer region’. The velocity profile near the wall is determined to be linear by means of enhanced wall treatment and the logarithmic wall function. The fluctuations of the dispersed vapor phase in nucleate boiling flow are due to the low density of vapor which is affected by the continuous liquid phase.

## 4 Results and discussion

In this paper, the effects of different parameters of two-phase flow evaporation with the heat and mass transfer mechanism during the phase change in a vertical tube is simulated numerically. The results of these conditions are investigated for water flow as the working fluid and the effect of gravity is taken into account. A low-Reynolds number form of the SST  $K - \omega$  model is used for turbulence modeling throughout the entire computation domain for the liquid and vapor phases.

### 4.1 Grid independency

In this section, it is aimed to explain the grid independency test. Six different two dimensional structured grids were considered for this goal. The finest grid has 48,000 cells. Vapor void fraction at outlet of the tube was considered to compare other coarser grids with the finer one. The relative error can be seen in Fig. 2. It is worth noting that the grids are finer in the wall adjacency to ensure the accuracy of the VOF method. As can be seen in the figure, the difference between the values of vapor void fraction of the case with 48,000 cells and that with 32,000 cells was less than 0.5%. Consequently, the solution is grid independent and the case with 32,000 cells was used for all simulations.

### 4.2 Comparison with experimental results

In order to evaluate the evaporation heat transfer coefficient of surface, a verification of the numerical simulation is carried out by experimental study of upward water flow boiling in a vertical tube [31]. The bore, outer diameter and tube length are 9, 12 and 280 mm, respectively. The results are obtained for

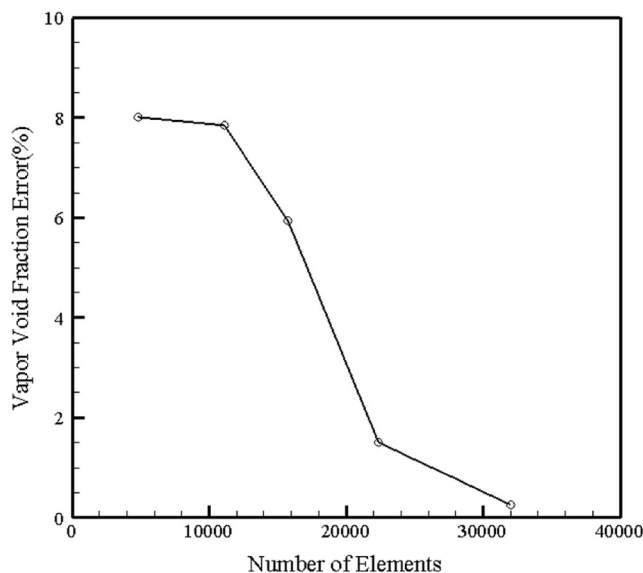


Fig. 2 Grid independency test results

steady state. The mass flux of 151 ( $\text{kg}/\text{m}^2\text{-s}$ ) and inlet sub-cooling of  $20^\circ\text{C}$  and wall heat flux of  $182 (\text{kW}/\text{m}^2)$  is considered. The comparison between the numerical results and experimental data is shown in Fig. 3, in which the heat transfer coefficient is investigated according to the numerical simulation approach. The jump in heat transfer coefficient is due to the variation of thermal conductivity and velocity difference between the liquid and vapor phases created on the heated wall. The vapor velocity near the surface is raised because of liquid-vapor interface on the control volume as a result of the evaporation. The velocity of vapor phase is increased compared to the liquid phase due to phase change and agitation of vapor bubbles which creates vortex flow near the heated surface [5]. Finally, good agreement between the results of the present study and the previous work can be observed that

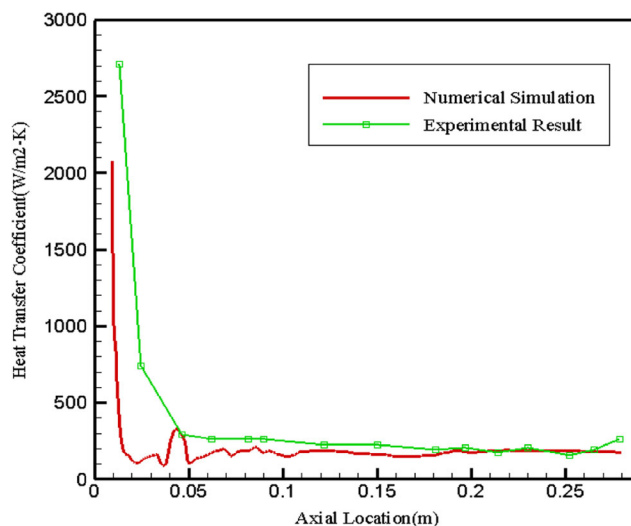
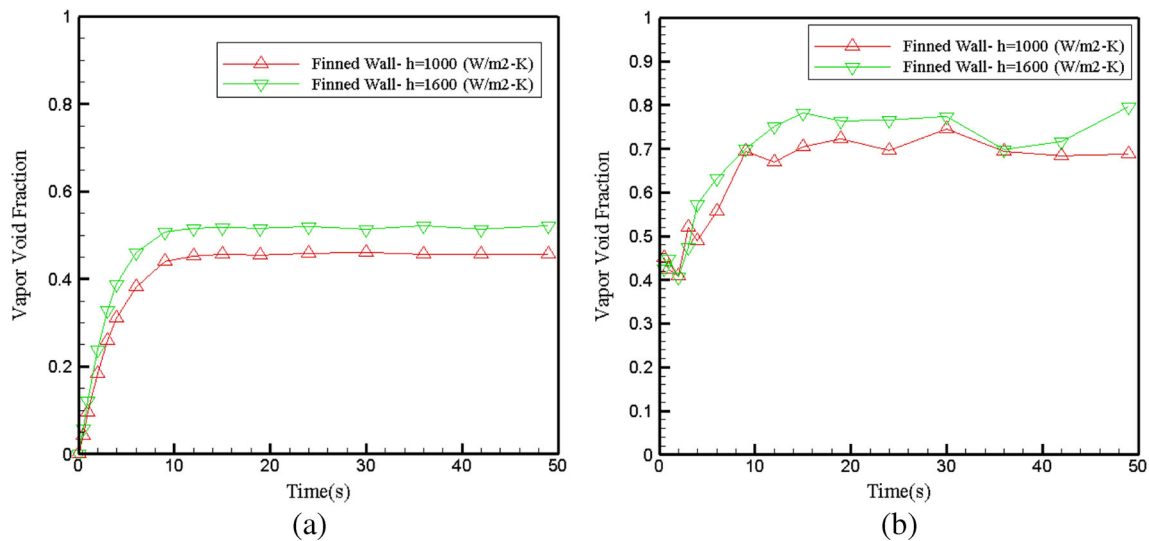


Fig. 3 Comparison of the numerical simulation results with the experimental data



**Fig. 4** (a): Volume average of vapor void fraction with time for two different convective boundary conditions. (b): Tube outlet vapor void fraction with time for two different convective boundary conditions

assures reliability of the results. The discrepancy between experimental and numerical analysis shows satisfactory results. Differences in the values of measurement results on the entrance of the flow are due to the dynamic behavior of two phase flow phenomena.

### 4.3 Effect of fin on the tube wall

In this section it is aimed to investigate the effect of wall convective boundary condition on vapor void fraction variations in the tube. Two cases of  $h = 1000 \text{ W/m}^2\text{-K}$  and  $h = 1600 \text{ W/m}^2\text{-K}$  were considered. Based on the tube and fin geometrical parameters as well as the industrial HRSG flue gas features, these two values of convective heat transfer coefficients are obtained using Ref. [32]. Tube diameter is 3.81 cm and the fluid flows with constant mass flow rate of 0.0477 kg/s. As mentioned previously, these two convective

boundary conditions correspond to the exhaust gases of a gas turbine that impinges to the finned tube bundles of a HRSG. Total length of the tube is under the effect of the fin. In both cases the tube is finned and obviously, the greater convective heat transfer coefficient ( $h = 1600 \text{ W/m}^2\text{-K}$ ) corresponds to the tube with extended fin size (20% extension in fin size) due to more energy exchange with the hot gas.

Figure 4a, shows the volume average of vapor void fraction in tube from  $t = 0.5 \text{ s}$  to  $t = 49 \text{ s}$ . It can be seen that the value of vapor in tube increases from zero to a constant value. This constant value is totally different for these two tubes of various fin size, i.e. 0.45 and 0.50. As expected, more quantities of vapor void fraction is obtained as the convective heat transfer increases on the heated wall. It can be seen that after about 10 s both of the diagrams reach to their steady state. It should be mentioned that this steady response is not constant with time but the variables seem to oscillate chaotically around a steady-

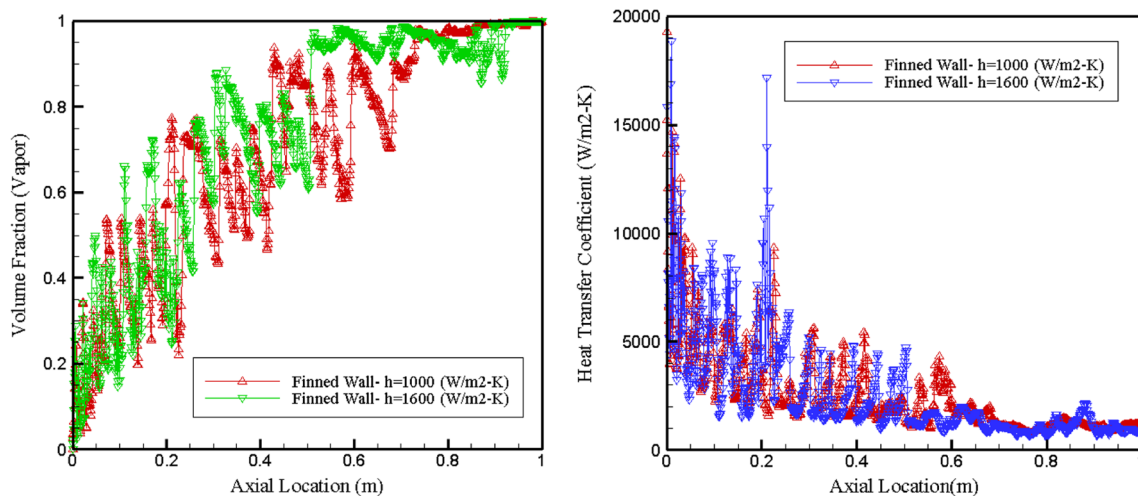


**Fig. 5** Comparison of void fraction and heat transfer coefficient on the heated wall at the time  $t = 36 \text{ s}$  for two different convective boundary conditions

state. This oscillation can be observed in next diagrams. One of the most important parameters in boilers is the void fraction of vapor at the outlet of the tubes. To investigate the values of water vapor at tube's outlet, this parameter is depicted with time in Fig. 4b. Similarly, it is seen that the expansion of fin size leads to higher values of water vapor void fraction at tube's outlet corresponding to higher convective heat transfer on the tube wall.

Figure 5 shows the influence of void fraction and heat transfer coefficient due to the extension of 20% fin size on the heated wall at the time  $t = 36$  s. When the vapor bubbles are attached to the heated surface, the bubble agitation in the thermal boundary layer adjacent to the surface causes the fluctuations of void fraction on the heated wall. Therefore, the fluctuations of the vapor void fraction on the surface are caused by interface of liquid-vapor two-phase flow while the small bubbles have a higher pressure than the large bubbles due to the surface tension [4]. The results show that the heat transfer coefficient values are averagely slightly lower than the previous mode when the fin size is extended, since the heat transfer coefficient of fluid is decreased due to the increase of vapor volume fraction. Furthermore, the behavior of the heat transfer coefficient is comparable to the formed vapor on the heated wall, therefore the fluctuating pattern found on the liquid-vapor phase can be seen in heat transfer coefficient diagram.

In Fig. 6 the values of vapor void fraction is depicted along the fluid flow path from tube's inlet ( $z = 0$ ) to its outlet ( $z = 1$  m). Mass weighted average of void fraction is obtained every 5 cm from inlet to outlet along the tube at different instances of time. As can be seen, the diagrams have oscillating behavior with a definite pattern. As the fluid flows through the tube, the void fraction of water vapor increases due to increment of fluids absorbed energy. Furthermore, at the beginning of tube's length, the oscillations are severe due to the development of flow and higher turbulence intensities. These diagrams show that at each instance of time, void fraction values can change and oscillate around a steady state. The pattern of the graph is partly the same at times greater than 9 s for both cases of  $h = 1000$  W/m<sup>2</sup>-K and  $h = 1600$  W/m<sup>2</sup>-K which is in accordance with the results of Fig. 4a.

#### 4.4 Effect of diameter variations

In this part, the effect of variations of tube diameter is considered at constant fluid mass flow rate of 0.0477 kg/s and convective heat transfer coefficient of  $h = 1000$  W/m<sup>2</sup>-K. Three different tube diameters of 2.54, 3.81 and 5.08 cm are considered for this purpose.

In Fig. 7a, the volume average of vapor void fraction is depicted with time. It is obvious that this parameter reaches to its steady state at about 4, 10 and 20 s for tube with diameters of 2.54, 3.81 and 5.08 cm, respectively. This difference

in the time in which the flow reaches to its steady state is due to the fact that the mass flow rate is constant and the flow has higher values of velocities in tubes with smaller diameters and therefore it gets steady faster than the tubes with greater diameters. This fact can be useful whenever the transient behavior of the flow is of high importance. It can also be seen that at constant mass flow rate, as the diameter of tube increases, the vapor void fraction enhances and the value of vapor in tube increases from zero to a constant value. This constant value is different for these three various tubes diameter, i.e. 0.30, 0.45 and 0.53 for tube with diameters of 2.54, 3.81 and 5.08 cm, respectively. As mentioned before this steady state is not constant with time but the variables seem to oscillate around a steady-state. The increment of vapor void fraction in tubes with greater diameters can be attributed to the fact that as the diameter and hence the contact area of the fluid increases, the flow obtains higher values of thermal energy from the turbine's exhaust gases impinging to it and therefore more water liquid is changed to water vapor. Figure 7b shows the average values of water vapor at tube's outlet with time. As stated, the values of water vapor void fraction at tube's outlet increases corresponding to greater tube diameters.

In Fig. 8 comparison of void fraction and heat transfer coefficient on the heated wall is shown for three different tube diameters at  $t = 36$  s. The unsteady behavior of the fluid can easily be seen in both diagrams of vapor void fraction and convective heat transfer coefficient. Although at chosen time, i.e.  $t = 36$  s the transient response of the flow has decayed but this oscillation is due to the transient nature of the flow. Therefore rational discussion of the flow behavior in one instant of time is impossible since the flow features can be different at a moment later due to the unsteady nature of the flow. Therefore the flow characteristics should be investigated at different moments of time.

In Fig. 9 vapor void fraction with axial location can be seen for three different tube diameters. The diagrams have oscillating behavior with a definite pattern. As the flow flows through the tube, the void fraction of water vapor increases due to increment of fluids absorbed energy and as mentioned previously at the beginning of tube's length these oscillations are higher. The pattern of the diagram becomes rather unchanged as the flow reaches to its so called oscillating steady state.

## 5 Conclusions

Numerical simulation of two-phase flow evaporation in a vertical tube is carried out using FVM method by employing the VOF model while the energy and mass transfer mechanism during the phase change has been taken into consideration. The conditions are investigated for water upward flow as the working fluid. The influence of various parameters of the case study such as convection boundary condition and diameter



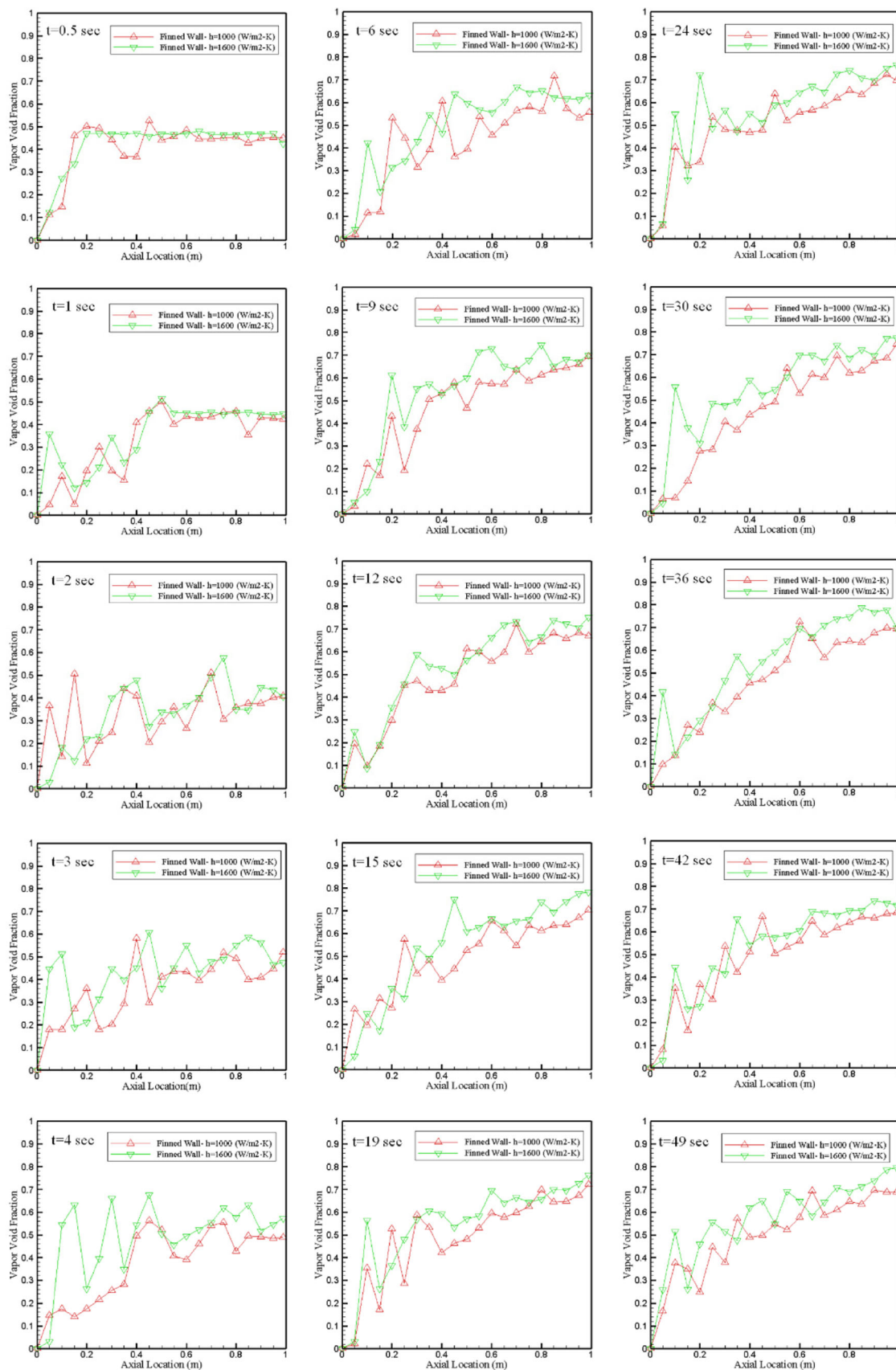
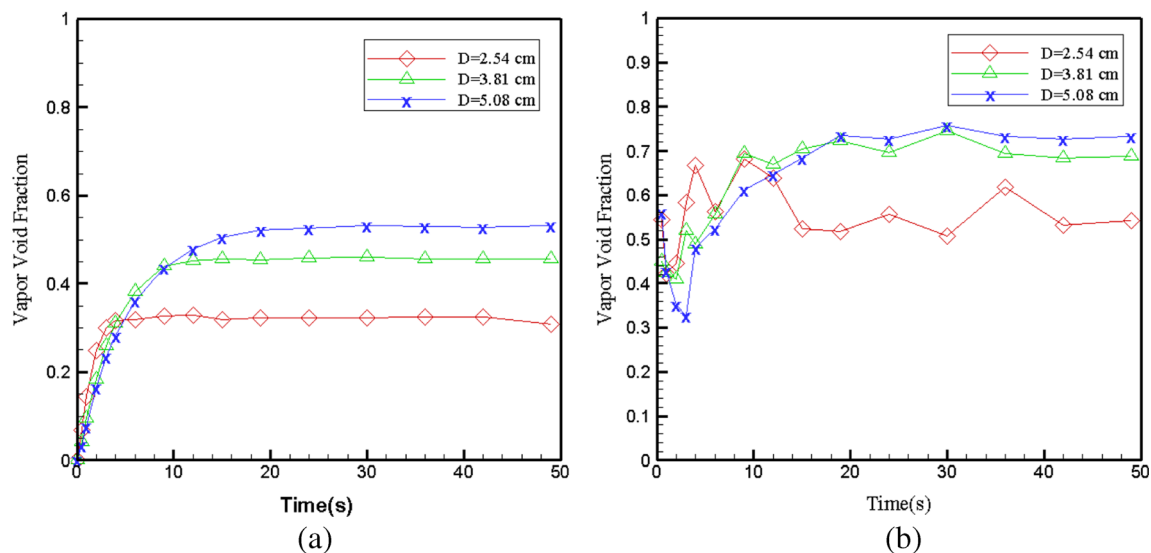


Fig. 6 Vapor void fraction with axial location for two different convective boundary conditions



**Fig. 7** (a): Volume average of vapor void fraction with time for three different tube diameters. (b): Tube outlet vapor void fraction with time for three different tube diameters

variations is investigated on the volume fraction and heat transfer coefficient. A CFD code with a UDF as a source term is accomplished during the phase change interaction throughout the entire computation domain for the liquid and vapor phases. The simulation of turbulent flow is based on standard  $K-\omega$  model as a modified formulation of the Shear-Stress Transport (SST). In order to improve the computational efficiency, the PISO algorithm is employed in comparison to the SIMPLE and SIMPLEC algorithms. Therefore, the continuity and volume fraction equations are implemented using the pressure interpolation with the PRESTO scheme and the modified HRIC scheme, respectively. The set of these parametric studies were developed to investigate heat transfer behavior on the tube layout and fin geometry which is conducted by diameter variation, convection boundary condition and mass flow rate variation.

The average of fluid heat transfer coefficient acquired from the numerical simulation was compared with the experimental data and a good agreement was observed. The main conclusions can be summarized as follows:

- The numerical approach used in the study results in a reasonable agreement compared to the experimental results for two phase flow boiling of water in a vertical tube.
- The fluctuations of vapor void fraction and heat transfer coefficient on the heated wall are caused by interaction of phases within a computational cell. Moreover, there is no fluctuation when the computational cell is filled with a single phase.
- The thermal conductivity variations and velocity difference between the liquid-vapor phases created on the heated wall is transmitted to the heat transfer coefficient and

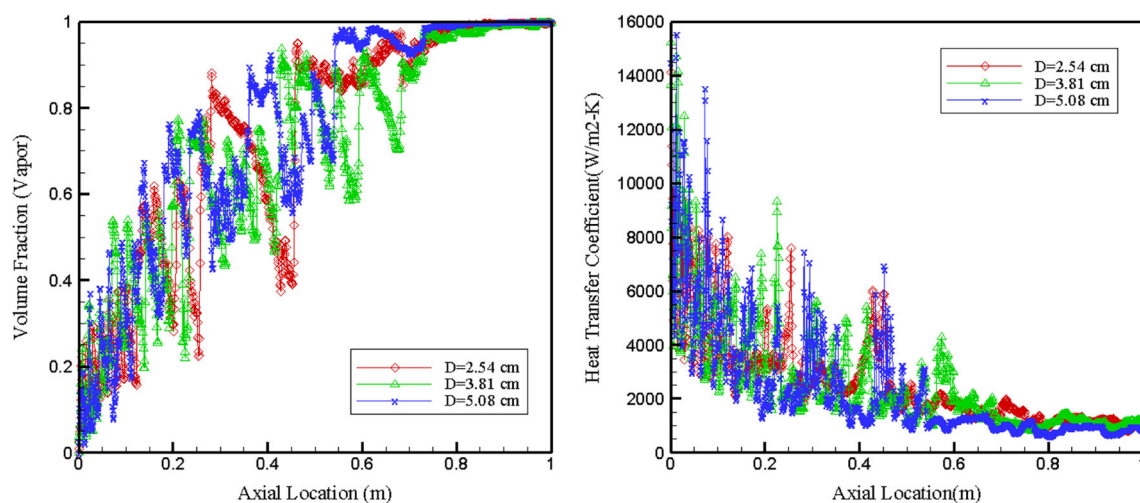


**Fig. 8** Comparison of void fraction and heat transfer coefficient on the heated wall at the time  $t = 36$  s for three different tube diameters

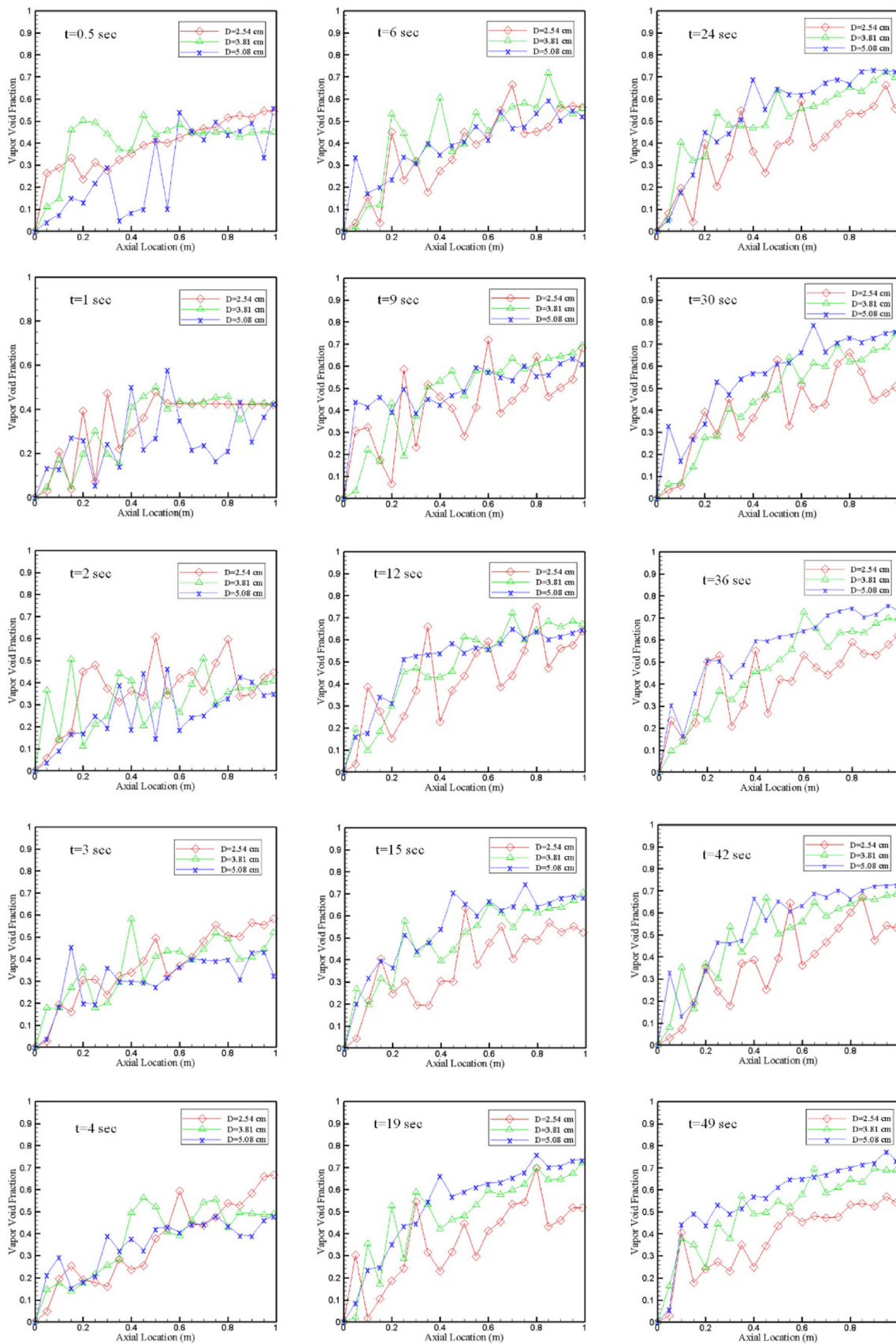


Fig. 9 Vapor void fraction with axial location for three different tube diameters

vapor void fraction. Due to agitation of vapor phase and vortex flow near the heated wall, the vapor velocity is intensified compared to the liquid phase as a consequence of the evaporation.

- Due to an increase in vapor void fraction values, the fluid heat transfer coefficient is decreased on the heated wall in which the heat transfer coefficient values are averagely lower than the previous mode when the fin size is extended.
- In bigger tube diameter, vapor void fraction values on the heated wall are more than the smaller one in which there is no fluctuation when the computational cell is filled with a single phase. Furthermore, the jump and oscillating behavior in void fraction and heat transfer coefficient on the heated wall is affected by the liquid-vapor phase properties.

## References

1. Yang Z, Peng X, Ye P (2008) Numerical and experimental investigation of two phase flow during boiling in a coiled tube. *Int J Heat Mass Transf* 51:1003–1016
2. Zambrana J, Leo T, Perez-del-Notario P (2008) Vertical tube length calculation based on available heat transfer coefficient expressions for the subcooled flow boiling region. *Appl Therm Eng* 28:499–513
3. Fang C, David M, Rogacs A, Goodson K (2010) Volume of fluid simulation of boiling two-phase flow in a vapor-venting microchannel. *Front Heat Mass Transfer* 1
4. Wei J, Pan L, Chen D, Zhang H, Xu J, Huang Y (2011) Numerical simulation of bubble behaviors in subcooled flow boiling under swing motion. *Nuclear Eng Des* 241:2898–2908
5. Kouhikamali R, Hassanpour B, Javaherdeh K (2012) Numerical simulation of forced convective evaporation in thermal desalination units with vertical tubes. *Desalin Water Treat*
6. Park, Seouk I (2010) Numerical analysis for flow, heat and mass transfer in film flow along a vertical fluted tube. *Int J Heat Mass Transf* 53:309–319
7. Chen Q, Xu J, Sun D, Cao Z, Xie J, Xing F (2013) Numerical simulation of the modulated flow pattern for vertical upflows by the phase separation concept. *Int J Multiphase Flow* 56:105–118
8. Ma C, Bothe D (2013) Numerical modeling of thermocapillary two-phase flows with evaporation using a two-scalar approach for heat transfer. *J Comput Phys* 233:552–573
9. Ratkovich N, Majumder S, Bentzen T (2012) Empirical correlations and CFD simulations of vertical two-phase gas–liquid (Newtonian and non-Newtonian) slug flow compared against experimental data of void fraction. *Chem Eng Res Des*
10. Meng M, Yang Z, Duan Y, Chen Y (2013) Boiling flow of R141b in vertical and inclined Serpentine Tubes. *Int J Heat Mass Transf* 57: 312–320
11. Liu Y, Cui J, Li W (2011) A two-phase, two-component model for vertical upward gas–liquid annular flow. *Int J Heat Fluid Flow* 32: 796–804
12. Liu Y, Li W, Quan S (2011) A self-standing two-fluid CFD model for vertical upward two-phase annular flow. *Nucl Eng Des* 241: 1636–1642
13. Vazquez-Ramirez E, Riesco-Avila J, Polley G (2013) Two-phase flow and heat transfer in horizontal tube bundles fitted with baffles of vertical cut. *Appl Therm Eng* 50:1274–1279
14. Maqbool M, Palm B, Khodabandeh R (2013) Investigation of two phase heat transfer and pressure drop of propane in a vertical circular minichannel. *Exp Thermal Fluid Sci* 46:120–130
15. Chiapero E, Ferdinando M, Dorao C (2014) Experimental results on boiling heat transfer coefficient, frictional pressure drop and flow patterns for R134a at a saturation temperature of 34 °C. *Int J Refrig* 40:317–327
16. Tsui Y, Lin S (2016) Three-dimensional modeling of fluid dynamics and heat transfer for two-fluid or phase change flows. *Int J Heat Mass Transf* 93:337–348
17. Hardt S, Wondra F (2008) Evaporation model for interfacial flows based on a continuum-field representation of the source terms. *J Comput Phys* 227:5871–5895
18. Pan Z, Weibel J, Garimella S (2016) A saturated-interface-volume phase change model for simulating flow boiling. *Int J Heat Mass Transf* 93:945–956
19. Kafeel K, Turan A (2013) Axi-symmetric simulation of a two phase vertical thermosyphon using Eulerian two-fluid methodology. *Heat Mass Transf* 49:1089–1099
20. Lorstad D, Fuchs L (2004) High-order surface tension VOF-model for 3D bubble flows with high density ratio. *J Comput Phys* 200: 153–176
21. Das A, Das P (2015) Modeling of liquid–vapor phase change using smoothed particle hydrodynamics. *J Comput Phys* 303:125–145
22. Collier J, Thome J (1994) *Convective Boiling and Condensation*. Clarendon Press, Oxford
23. Lakehal D, Meier M, Fulgosi M (2002) Interface tracking towards the direct simulation of heat and mass transfer in multiphase flows. *Int J Heat Fluid Flow* 23:242–257
24. Lorstad D, Francois M, Shyy W, Fuchs L (2004) Assessment of volume of fluid and immersed boundary methods for droplet computations. *Int J Numer Methods Fluids* 46:109–125
25. Benson, David J (2002) Volume of fluid interface reconstruction methods for multi-material problems. *Appl Mech Rev* 55(2):151–165
26. Brackbill J, Kothe D, Zemach C (1992) A continuum method for modeling surface tension. *J Comput Phys* 100:335–354
27. Just T, Kelm S (1986) *Die Industry*, pp 38–76
28. Issa R (1985) Solution of the implicitly discretized fluid flow equations by operator-splitting. *J Comput Phys* 62:40–65
29. Versteeg H, Malalasekera W (2007) *An Introduction to Computational Fluid Dynamics*, Second edition ed., Pearson Education Limited
30. Menter F, Kuntz M, Langtry R (2003) Ten Years of industrial Experience with the SST Turbulence Model. *Turbul Heat Mass Transf* 4:625–632
31. Mosaad M, Johannsen K (1989) Experimental Study of Steady-State Film Boiling Heat Transfer of Subcooled Water Flowing Upwards in a Vertical Tube. *Exp Thermal Fluid Sci* 2:477–493
32. Kawaguchi K, Okui K, Asai T, Hasegawa Y (2006) The heat transfer and pressure drop characteristics of the finned tube banks in forced convection (Effect of fin height on heat transfer characteristics). *Heat Transfer-Asian Res* 35(3):194–208